International Journal of Analysis and Applications

Mathematical Investigation of Non-Linear Reaction-Diffusion Equations on Multiphase Flow Transport in the Entrapped-Cell Photobioreactor Using Asymptotic Methods

A. Reena, R. Swaminathan*

PG & Research Department of Mathematics, Vidhyaa Giri College of Arts and Science (Affiliated to Alagappa University), Puduvayal-630108, Tamil Nadu, India

**Corresponding author:* swaminathanmath@gmail.com

ABSTRACT. The mathematical investigation of a multiphase flow transport model intended to clarify the interaction mechanism between reactions and diffusion processes in the gel granules containing the entrapped-cell photobioreactor Rhodopseudomonas palustris CQK 01 is presented in this research. The model uses two pertinent non-linear reaction-diffusion equations for biochemical interactions in the photobioreactor under steady-state circumstances to reflect the substrate and product concentration within the gel granules. The solid phase and liquid phase fluxes within the gel granules and their concentrations are analytically calculated using the asymptotic methods of the Akbari-Ganji method and the homotopy perturbation approach. Our analytical results and the numerical data obtained by MATLAB software are compared to determine accuracy. The analytical results agreed with the simulated results for all possible reaction-diffusion and saturation parameter values. In addition, the impacts of applying two limiting cases—saturated and unsaturated enzyme kinetics—were examined. The close correspondence between the simulated and analytical data demonstrates that the parameters in our suggested solution can be used to simulate the dynamic performance of a system.

1. Introduction

Sustainable energy is produced from resources that can support present activities without endangering the climate or the energy demands of future generations. Wind, solar, and

Received Mar. 14, 2024

2020 Mathematics Subject Classification. 34M30, 35A35, 97M60, 34B15.

Key words and phrases. asymptotic methods; non-linear reaction-diffusion equations; mathematical modelling; analytical solutions.

https://doi.org/10.28924/2291-8639-22-2024-74

ISSN: 2291-8639

hydropower are some of the most widely used renewable energy sources. The need for sustainable energy is rising due to the depletion of fossil fuels. Humans and the environment have suffered dramatically due to an over-reliance on fossil fuels. Hydrogen is frequently seen as an appealing replacement for fossil fuels because of its efficient conversion and clean burning, which produces no CO2. Biological hydrogen generation is a secure, affordable, and sustainable method of producing hydrogen owing to its environmental dependability, capability to prevent ecological damage, and inexpensive equipment investment costs [1,2]. Photosynthetic bacteria (PSB), one of the microorganisms used to produce biological hydrogen, is a feasible option due to its high theoretical considerations, changing yield, and ability to prevent the oxygen suppression of biological systems brought on by oxygen-evolving activity [3]. In addition, PSB can treat waste by biodegrading a wide range of organic substrates and a broad spectrum of solar radiation [4]. As a result, this topic has attracted the attention of numerous researchers worldwide.

Many experiments on PSB photohydrogen generation are currently being conducted in the suspended-cell photobioreactor because of the excellent mass transfer. The potential to repair and reuse cell mass and advances in cell concentration and operational stability make techniques for immobilizing cells, including biofilm, cell entrapment, and self-flocculation, promising [5]. Particularly, cell entrapment is a more rational approach because it can offer a steady and beneficial environment for the growth of PSB trapped by gel granules. In the entrapped-cell photobioreactor, it is essential to note that multiphase flow, mass transfer, and biochemical reactions all coincide. This has an impact on the features of the substrate concentration distribution and the efficiency of photo-hydrogen production. Therefore, it is advantageous to encourage the scale-up use of photo-hydrogen generation systems by providing complete analyses of the intricate biochemical responses and transport processes. However, it is exceedingly challenging to experimentally assess the multiphase flow and mass transfer concerning the biochemical activities in the entrapped-cell photobioreactor.

The mathematical model is a potent tool that can explain how biochemical reactions and transfer mechanisms interact. Numerous mathematics models have been developed recently to forecast the creation of photohydrogen. The characteristics of Rhodopseudomonas palustris CQK 01's substrate consumption and hydrogen production in an immobilized-cell photobioreactor were examined by Wang et al. [6,7]. An innovative annular fiber-illuminating biological

hydrogen reactor was investigated as part of a two-dimensional steady-state model developed by Zhang et al. to simulate substrate degradation and diffusion in the biofilm zone and substrate convection and distribution in the bulk fluid zone [8,9]. Yang et al. [10] used the lattice Boltzmann method to model a biological reaction in a substrate solution passing around a circular cylinder. Liao et al. [11] developed a two-phase flow and mass transfer model to forecast the production of photohydrogen and substrate biodegradation. Guo et al. [12] conducted a simulation study to examine the features of photo-hydrogen generation and substrate deterioration across different stacking configurations.

Even if we have numerical solutions for every type of model, a thorough analysis of the system requires identifying the analytical solution. Recently, there has been a lot of focus on determining the reaction-diffusion equations' straightforward approximation analytical expression. Ganji et al. [13] used He's Energy Balance Method to derive approximations of solutions. Two methods are employed in the mathematical model of two-phase flow transfer in an immobilized-cell photobioreactor: the homotopy perturbation approach by Shirejini et al. [14] and the Adomian decomposition method by Praveen et al. [15]. Using Bernoulli Wavelets and a spectral method, Venkata Subrahmanyam Sajja et al. [16] solved reaction-diffusion equations in gel-granules. The problem based on electroactive polymer film placed on an inlaid micro disc electrode was solved analytically by Meena and Rajendran using HPM [17]. Jeyabharathi et al. used Akbari-Ganji and Taylor's series methodology to develop a packed bed immobilized-cell electrochemical photobioreactor [18].

Guo et al. outlined a multiphase mixture model for the entrapped-cell photobioreactor's photo-hydrogen generation performance and substrate concentration distribution features [19]. An analytical solution for the multiphase mixture model has yet to be published. In the current work, the homotopy perturbation approach and the Akbari-Ganji method are used to derive the analytical solution for a multiphase mixture model for the concentrations of substrate, hydrogen production, solid and liquid phase flows in the entrapped-cell photobioreactor. Furthermore, the effects of reaction-diffusion and saturation parameters on substrate (glucose) and product (hydrogen) concentrations are also investigated.

2. Model construction and analysis

Guo et al. [19] designed a cell-photobioreactor that is entrapped and filled with gel granules carrying PSB (Rhodopseudomonas palustris CQK 01), as shown in Fig. 1. The h-direction refers

to the substrate flow direction in the primary channel, and the r-direction relates to the product transport direction inside the gel granule. The entrapped-cell photobioreactor's peristaltic pump provides the substrate medium, and the only carbon source used is glucose. Once the glucose has diffused into gel granules from the primary channel, the entrapped cells biodegrade it. The produced gases and metabolites eventually diffuse out of the gel granules under the flow of the substrate medium in the entrapped-cell photobioreactor. Evidently, in the entrapped-cell photobioreactor, multiphase flow, biochemical reactions and mass transfer all coincide.

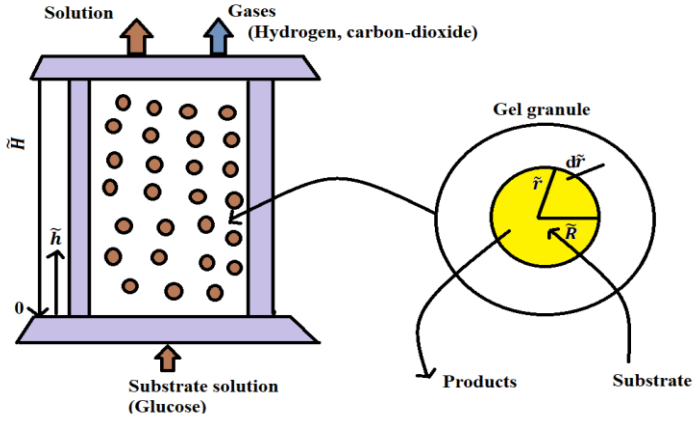

FIGURE 1. Schematic representation of the entrapped-cell photobioreactor.

The model's development takes into account the following presumptions. Operating conditions for the entrapped-cell photobioreactor are steady-state. The substrate and product transfer processes are viewed as a one-dimensional flow along the h-direction in the significant channel. Darcy's law can be used to describe substrate and product transfer processes because it assumes that fluids' physical and thermal properties stay constant. The biochemical processes are limited to gel granules. The PSB's consistent distribution and activity within the gel granules are considered. The mole ratio of carbon dioxide to hydrogen, the sole gaseous product produced by substrate biodegradation, is 2:1 [20].

In the entrapped-cell photobioreactor, it is anticipated that the multiphase mixture model can adequately represent the processes of mass transfer and multiphase flow in the gel granules. Diffusion is crucial in the reactant and the product's mass movement. Applying Fick's law, the mass transfer equation for the substrate and hydrogen inside the gel granules is as follows [19]:

$$D_{Gr}^{\tilde{S}} \frac{d^2 C_{Gr}^{\tilde{S}}}{d\tilde{r}^2} + \frac{2D_{Gr}^{\tilde{S}}}{\tilde{r}} \frac{dC_{Gr}^{\tilde{S}}}{d\tilde{r}} = \frac{\varphi_{Gr}^{\tilde{S}}}{K_1} \tag{2.1}$$

$$D_{Gr}^{\widetilde{H_2}} \frac{d^2 C_{Gr}^{\widetilde{H_2}}}{d\tilde{r}^2} + \frac{2D_{Gr}^{\widetilde{H_2}}}{\tilde{r}} \frac{dC_{Gr}^{\widetilde{H_2}}}{d\tilde{r}} = \frac{\varphi_{Gr}^{\widetilde{H_2}}}{K_2} \tag{2.2}$$

Here,

$$\varphi_{Gr}^{\tilde{S}} = \left(\frac{1}{\tilde{Y}_{\frac{X}{S}}}\tilde{\mu} + \tilde{m}\right)\tilde{\Psi}\widetilde{C^c}\ , \varphi_{Gr}^{\widetilde{H_2}} = \left(\frac{\widetilde{\alpha^*}}{\tilde{Y}_{\frac{X}{S}}}\tilde{\mu} + \tilde{\beta}\right)\tilde{\Psi}\widetilde{C^c},$$

$$\tilde{m} = 0.562137\exp\left(-5.1\left(\frac{\widetilde{pH}}{7-1}\right)^2\right)\exp\left(-4.5\left(\frac{\tilde{T}}{30-1}\right)^2\right), \tilde{\mu} = \tilde{\mu}_{max}\frac{C_{Gr}^{\tilde{S}}}{K_{\tilde{S}}+C_{Gr}^{\tilde{S}}},$$

$$\tilde{\mu}_{max} = 0.25986\exp\left(-10.8\left(\frac{\widetilde{pH}}{7-1}\right)^2\right) - 10.5\left(-4.5\left(\frac{\tilde{T}}{30-1}\right)^2\right),$$

$$\delta = 0.0192\exp\left(-21.2\left(\frac{\widetilde{pH}}{7-1}\right)^2\right) - 8.1\left(-4.5\left(\frac{\tilde{T}}{30-1}\right)^2\right) \quad (2.3)$$

The concentrations of substrate and hydrogen in the gel granules are represented by $C_{Gr}^{\tilde{S}}$ and $C_{Gr}^{\widetilde{H_2}}$. For substrate and hydrogen in the gel granules; their corresponding effective diffusion coefficients are $D_{Gr}^{\tilde{S}}$ and $D_{Gr}^{\widetilde{H_2}}$. The substrate biodegradation rate for PSB trapped in the gel granules is indicated by $\varphi_{Gr}^{\tilde{S}}$, whereas the hydrogen production rate is represented by $\varphi_{Gr}^{\widetilde{H_2}}$. The specific growth rate of PSB and the maintenance coefficient are denoted by the symbols $\tilde{\mu}$ and $\tilde{m}$, respectively; $\tilde{\Psi}$ is the cell density increasing coefficient, and $\widetilde{C^c}$ is the cell density. $\tilde{Y}_{\frac{X}{S}}$ represents the cell yield, The monod constant is $K_{\tilde{S}}$, the operation temperature is $\tilde{T}$, and $\widetilde{pH}$ stands for the medium pH values. $\tilde{\mu}_{max}$ is the highest possible specific growth rate. For hydrogen production, $\tilde{\beta}$ is the non-growth-associated kinetic constant, and δ is the growth-associated kinetic constant. $K_1$and K_2 represents the molecular weight of glucose and hydrogen respectively. The value of $\widetilde{pH}$ and $\tilde{T}$ are considered to be 7 and 30℃ according to the experimental data.

The corresponding boundary conditions for the dimensional Eqs. (2.1) and (2.2) are listed below:

$$\tilde{r} = 0, \frac{dC_{Gr}^{\tilde{S}}}{d\tilde{r}} = 0; \frac{dC_{Gr}^{\widetilde{H_2}}}{d\tilde{r}} = 0 \quad (2.4)$$

$$\tilde{r} = \tilde{R}, C_{Gr}^{\tilde{S}} = C_l^{\tilde{S}}\ ; C_{Gr}^{\widetilde{H_2}} = C_g^{\widetilde{H_2}} \quad (2.5)$$

The bulk solutions are $C_l^{\tilde{S}}$ and $C_g^{\widetilde{H_2}}$, whereas $\tilde{R}$ represents the catalyst's radius.

The system of equations (2.1) and (2.2) can be simplified by defining the following variables to transform it into a dimensionless form:

$$\varphi_1 = \frac{\tilde{R}^2\tilde{\mu}_{max}\tilde{\Psi}\widetilde{C^c}}{\tilde{Y}_{\frac{X}{S}}D_{Gr}^{\tilde{S}}K_{\tilde{S}}}, \varphi_2 = \frac{\delta\tilde{R}^2\tilde{\mu}_{max}\tilde{\Psi}\widetilde{C^c}C_l^{\tilde{S}}}{\tilde{Y}_{\frac{X}{S}}D_{Gr}^{\widetilde{H_2}}K_{\tilde{S}}C_g^{\widetilde{H_2}}}, \alpha_1 = \frac{\tilde{R}^2\tilde{m}\tilde{\Psi}\widetilde{C^c}}{D_{Gr}^{\tilde{S}}C_l^{\tilde{S}}}, \alpha_2 = \frac{\tilde{R}^2\tilde{\beta}\tilde{\Psi}\widetilde{C^c}}{D_{Gr}^{\widetilde{H_2}}C_g^{\widetilde{H_2}}}, \gamma = \frac{C_l^{\tilde{S}}}{K_{\tilde{S}}}, U = \frac{C_{Gr}^{\tilde{S}}}{C_l^{\tilde{S}}},$$

$$V = \frac{C_{Gr}^{\widetilde{H_2}}}{C_g^{\widetilde{H_2}}}, \varepsilon = \frac{\tilde{r}}{\tilde{R}} \quad (2.6)$$

By applying Eq. (2.6) in (2.1) and (2.2), the equations' dimensionless form becomes:

$$\frac{d^2U(\varepsilon)}{d\varepsilon^2}+\frac{2}{\varepsilon}\frac{dU(\varepsilon)}{d\varepsilon}=\frac{1}{K_1}\left[\frac{(\varphi_1)U(\varepsilon)}{(1+\gamma U(\varepsilon))}+\alpha_1\right] \tag{2.7}$$

$$\frac{d^2V(\varepsilon)}{d\varepsilon^2}+\frac{2}{\varepsilon}\frac{dV(\varepsilon)}{d\varepsilon}=\frac{1}{K_2}\left[\frac{(\varphi_2)U(\varepsilon)}{(1+\gamma U(\varepsilon))}+\alpha_2\right] \tag{2.8}$$

The associated boundary conditions would change to:

$$\frac{dU}{d\varepsilon}=\frac{dV}{d\varepsilon}=0 \text{ when } \varepsilon=0 \tag{2.9}$$

$$U=V=1 \text{ when } \varepsilon=1 \tag{2.10}$$

Thus, in the entrapped-cell photobioreactor, the substrate biodegradation rate $\emptyset^{\tilde{S}}$ can be determined by:

$$\emptyset^{\tilde{S}}=\tilde{\alpha}K_1D_{Gr}^{\tilde{S}}\frac{dC_{Gr}^{\tilde{S}}}{d\tilde{r}}\Big|_{\tilde{r}=\tilde{R}} \tag{2.11}$$

Where α is the elemental volume's specific gel granule area.

Furthermore, the gas and liquid phase interfacial mass transfer rate can be written as follows:

$$\widetilde{m}_l=-\emptyset^{\tilde{S}} \tag{2.12}$$

$$\widetilde{m}_g=\emptyset^{\widetilde{H_2}}+\emptyset^{\widetilde{CO_2}} \tag{2.13}$$

Where the rates of generation of hydrogen and carbon dioxide, respectively, are denoted by $\emptyset^{\widetilde{H_2}}$ and $\emptyset^{\widetilde{CO_2}}$, which can be defined as:

$$\emptyset^{\widetilde{H_2}}=\tilde{\alpha}K_2D_{Gr}^{\widetilde{H_2}}\frac{dC_{Gr}^{\widetilde{H_2}}}{d\tilde{r}}\Big|_{\tilde{r}=\tilde{R}} \tag{2.14}$$

$$\frac{2\emptyset^{\widetilde{CO_2}}}{K_3}=\frac{\emptyset^{\widetilde{H_2}}}{K_2} \tag{2.15}$$

Here, K_3 denotes the molecular weight of carbon dioxide.

The following gives the expressions for the liquid and gas phases under steady-state conditions:

$$\sigma_l=\frac{\widetilde{m}_l\tilde{R}}{\alpha D_{Gr}^{\tilde{S}}C_l^{\tilde{S}}}=-\frac{dU}{d\varepsilon}\Big|_{\varepsilon=1} \tag{2.16}$$

$$\sigma_g=\frac{\widetilde{m}_g\tilde{R}}{\alpha D_{Gr}^{\widetilde{H_2}}C_g^{\widetilde{H_2}}}=\frac{dV}{d\varepsilon}\Big|_{\varepsilon=1}\left(1+\frac{1}{2}\eta\right) \tag{2.17}$$

Where $\eta=\frac{K_3}{K_2}$.

3. Analytical expressions for concentrations and two phases using asymptotic methods

3.1 An approximative analytical expression for the concentration of the substrate and product using HPM

Recent techniques for solving non-linear differential equations include using hyperbolic functions [21-22], Taylor's series approach [23-24], Adomian decomposition method [25], the

homotopy analysis method [26], and variational iteration method [27]. Among these techniques, Ji-Huan's homotopy perturbation method (HPM) uses the linearization process to solve non-linear equations [28-30]. This method would find and add a small parameter to the equation, utilizing the traditional perturbation method while eliminating its limitations. Numerous studies have used HPM to formulate an analytical solution for non-linear equations in various engineering and physical problems [31-32]. This approach combines traditional perturbation techniques with the topological concept of homotopy. The current study uses the HPM and Akbari-Ganji approach to analytically approximate equations (2.7) and (2.8).

By utilizing the HPM on Eqs. (2.7) and (2.8), analytical computations were generated for the concentrations, liquid, and gas phases for every parameter value (Appendix-A).

$$U(\varepsilon) = 1 + \frac{(\gamma\alpha_1+\alpha_1+\varphi_1)(\varepsilon^2-1)}{6K_1(1+\gamma)} \tag{3.1}$$

$$V(\varepsilon) = 1 + \frac{(\gamma\alpha_2+\alpha_2+\varphi_2)(\varepsilon^2-1)}{6K_2(1+\gamma)} \tag{3.2}$$

$$\sigma_l = \frac{(-\gamma-1)\alpha_1-\varphi_1}{3K_1(1+\gamma)} \tag{3.3}$$

$$\sigma_g = \frac{(\alpha_2(1+\gamma)+\varphi_2)\left(1+\frac{\eta}{2}\right)}{3K_2(1+\gamma)} \tag{3.4}$$

3.2 Analytical solutions for the substrate and product concentrations utilizing the Akbari-Ganji method

M. Akbari and D. Ganji proposed the Akbari-Ganji method (AGM) which has been effectively employed for determining analytical solutions for non-linear equations. The Akbari-Ganji Method is the new name for this method, formerly known as the Algebraic Method. Recently, this technique was applied to solve a non-linear problem in the chemical sciences [33-35].

Using the AGM to solve equations (2.7) and (2.8), analytical computations were generated for the concentrations and source terms of the liquid and gas phases (Appendix-B).

$$U(\varepsilon) = \frac{\cosh(l\varepsilon)}{\cosh(l)} \tag{3.5}$$

$$V(\varepsilon) = \frac{\cosh(m\varepsilon)}{\cosh(m)} \tag{3.6}$$

$$\sigma_l = -\frac{dU}{d\varepsilon}\Big|_{\varepsilon=1} = -\frac{l\,sinh(l)}{cosh(l)} \tag{3.7}$$

$$\sigma_g = \frac{dV}{d\varepsilon}\Big|_{\varepsilon=1}\left(1+\frac{1}{2}\eta\right) = \frac{m\,sinh(m)}{cosh(m)}\left(1+\frac{1}{2}\eta\right) \tag{3.8}$$

4. Limiting cases

4.1 Analytical solutions for unsaturated enzyme kinetics

In this case, the gel-granule's substrate concentration, $C_l^{\tilde{S}}$, was lower than the Monod constant, $K_{\tilde{S}}$. This circumstance happened when $\gamma U \ll 1$. As a result, Eqs. (2.7) and (2.8) can be reduced to the following equations:

$$\frac{d^2U(\varepsilon)}{d\varepsilon^2} + \frac{2}{\varepsilon}\frac{dU(\varepsilon)}{d\varepsilon} - \frac{1}{K_1}[(\varphi_1)U(\varepsilon) + \alpha_1] = 0 \tag{4.1}$$

$$\frac{d^2V(\varepsilon)}{d\varepsilon^2} + \frac{2}{\varepsilon}\frac{dV(\varepsilon)}{d\varepsilon} - \frac{1}{K_2}[(\varphi_2)U(\varepsilon) + \alpha_2] = 0 \tag{4.2}$$

The coupled Eqs. (4.1) and (4.2) approximate analytical results for concentrations, liquid and gas phases are expressed as follows by applying the HPM and the AGM:

$$U(\varepsilon) = 1 + \frac{((\varphi_1+\alpha_1)(\varepsilon^2-1)}{6K_1} \tag{4.3}$$

$$V(\varepsilon) = 1 + \frac{((\varphi_2+\alpha_2)(\varepsilon^2-1)}{6K_2} \tag{4.4}$$

$$\sigma_l = \frac{-((\varphi_1+\alpha_1)}{3K_1} \tag{4.5}$$

$$\sigma_g = \frac{\varphi_2+\alpha_2(2+\eta)}{6K_2} \tag{4.6}$$

Eqs. (4.3) – (4.6) represents the analytical expressions obtained using the homotopy perturbation method.

The analytical expressions are derived as follows after using the AGM to solve the coupled equations of (4.1) and (4.2):

$$U(\varepsilon) = \frac{\cosh(n\varepsilon)}{\cosh(n)} \tag{4.7}$$

$$V(\varepsilon) = \frac{\cosh(k\varepsilon)}{\cosh(k)} \tag{4.8}$$

$$\sigma_l = -\frac{n\,sinh(n)}{cosh(n)} \tag{4.9}$$

$$\sigma_g = \frac{k\,sinh(k)}{cosh(k)}\left(1 + \frac{1}{2}\eta\right) \tag{4.10}$$

Where the constant coefficients n and k are obtained by solving these equations:

$$n^2 + 2\,n\tanh(n) - \frac{1}{K_1}[(\varphi_1)U(\varepsilon) + \alpha_1] = 0 \tag{4.11}$$

$$k^2 + 2\,k\tanh(k) - \frac{1}{K_2}[(\varphi_2)U(\varepsilon) + \alpha_2] = 0 \tag{4.12}$$

4.2 Analytical expressions with saturated kinetics

The limiting condition, where $\gamma U \gg 1$, occurs when the substrate utilization rate remains constant concerning the substrate concentration. The simplified equations of (2.7) and (2.8) can be defined below:

$$\frac{d^2U(\varepsilon)}{d\varepsilon^2} + \frac{2}{\varepsilon}\frac{dU(\varepsilon)}{d\varepsilon} - \frac{1}{K_1}\left[\frac{\varphi_1}{\gamma} + \alpha_1\right] = 0 \tag{4.13}$$

$$\frac{d^2V(\varepsilon)}{d\varepsilon^2} + \frac{2}{\varepsilon}\frac{dV(\varepsilon)}{d\varepsilon} - \frac{1}{K_2}\left[\frac{\varphi_2}{\gamma} + \alpha_2\right] = 0 \tag{4.14}$$

Analytical solutions by homotopy perturbation method:

$$U(\varepsilon) = 1 + \frac{((\varphi_1+\gamma\alpha_1)(\varepsilon^2-1)}{6\gamma K_1} \tag{4.15}$$

$$V(\varepsilon) = 1 + \frac{((\varphi_2+\gamma\alpha_2)(\varepsilon^2-1)}{6\gamma K_2} \tag{4.16}$$

$$\sigma_l = \frac{-((\varphi_1+\gamma\alpha_1)}{3\gamma K_1} \tag{4.17}$$

$$\sigma_g = \frac{\varphi_2+\gamma\alpha_2(2+\eta)}{6\gamma K_2} \tag{4.18}$$

Analytical expressions by Akbari-Ganji method:

$$U(\varepsilon) = \frac{\cosh(p\varepsilon)}{\cosh(p)} \tag{4.19}$$

$$V(\varepsilon) = \frac{\cosh(q\varepsilon)}{\cosh(q)} \tag{4.20}$$

$$\sigma_l = -\frac{p\,sinh(p)}{cosh(p)} \tag{4.21}$$

$$\sigma_g = \frac{q\,sinh(q)}{cosh(q)}\left(1 + \frac{1}{2}\eta\right) \tag{4.22}$$

After resolving these equations, the constant coefficients p and q can be determined:

$$p^2 + 2\,p\tanh(p) - \frac{1}{K_1}\left[\frac{\varphi_1}{\gamma} + \alpha_1\right] = 0 \tag{4.23}$$

$$q^2 + 2\,q\tanh(q) - \frac{1}{K_2}\left[\frac{\varphi_2}{\gamma} + \alpha_2\right] = 0 \tag{4.24}$$

5. Analytical results validation

Numerical techniques were utilized to solve the non-linear reaction-diffusion equations (2.7) and (2.8), along with the appropriate boundary conditions (2.9) and (2.10). The MATLAB software's pdex4 function, a tool for resolving boundary value issues for partial differential equations, was utilized to solve these equations numerically. There was a satisfactory level of agreement when comparing the numerical solutions with the HPM and AGM. Two iterations of the HPM and simple algebraic calculations of AGM were used to calculate the approximate

concentrations. The reader might initially conclude that the AGM yields more accurate results than the HPM. As we only used the zeroth and first-order iterations in the latter technique, remember that the accuracy can be significantly boosted if additional iterations are encountered. The overall relative error for the HPM is 0.42 %, and AGM is 0.25 % for the various reaction-diffusion parameter values (φ_1, φ_2) displayed in Tables 1 and 2.

Table 1. Comparison of the numerical simulation for the substrate concentration (U) with the analytical results of Eqs. (3.1) and (3.5) for various values of parameter φ_1.

ε	φ_1 = 0.1					φ_1= 3					φ_1 = 7				
	Num	**HPM Eq. (3.1)**	**HPM Error %**	**AGM Eq. (3.5)**	**AGM Error %**	**Num**	**HPM Eq. (3.1)**	**HPM Error %**	**AGM Eq. (3.5)**	**AGM Error %**	**Num**	**HPM Eq. (3.1)**	**HPM Error %**	**AGM Eq. (3.5)**	**AGM Error %**
0	0.9754	0.9753	0.01	0.9755	0.01	0.18	0.1754	2.56	0.18	0.00	0.5295	0.5278	0.32	0.5295	0.00
0.2	0.9764	0.9763	0.01	0.9765	0.01	0.2052	0.2022	1.46	0.2015	1.80	0.5465	0.5471	0.11	0.5465	0.00
0.4	0.9795	0.9793	0.02	0.9794	0.01	0.2872	0.2908	1.25	0.285	0.77	0.5985	0.6049	1.07	0.5984	0.02
0.6	0.9846	0.9844	0.02	0.9845	0.01	0.4412	0.4423	0.25	0.439	0.50	0.6868	0.7012	2.10	0.6889	0.31
0.8	0.9917	0.9914	0.03	0.9914	0.03	0.6845	0.686	0.22	0.6825	0.29	0.8127	0.8361	2.88	0.8235	1.33
1	1	1	0.00	1	0.00	1	1	0.00	1	0.00	1	1	0.00	1	0.00
Average error %			0.02		0.01			0.96		0.56			1.08		0.28

Table 2. Examine the numerical simulation for various reaction-diffusion parameter values φ_2 for product concentration (V) using eqns. (3.2) and (3.6).

ε	φ_2 = 1					φ_2 = 3					φ_2 = 7				
	Num	**HPM Eq. (3.2)**	**HPM Error %**	**AGM Eq. (3.6)**	**AGM Error %**	**Num**	**HPM Eq. (3.2)**	**HPM Error %**	**AGM Eq. (3.6)**	**AGM Error %**	**Num**	**HPM Eq. (3.2)**	**HPM Error %**	**AGM Eq. (3.6)**	**AGM Error %**
0	0.8895	0.8889	0.07	0.8868	0.30	0.8351	0.8333	0.22	0.835	0.01	0.7807	0.7778	0.37	0.787	0.81
0.2	0.894	0.8934	0.07	0.8913	0.30	0.8416	0.8401	0.18	0.8414	0.02	0.7897	0.7868	0.37	0.7964	0.85
0.4	0.9075	0.907	0.06	0.905	0.28	0.8612	0.8605	0.08	0.861	0.02	0.8167	0.8141	0.32	0.8206	0.48
0.6	0.9297	0.9296	0.01	0.9278	0.20	0.894	0.894	0.00	0.894	0.00	0.8632	0.8594	0.44	0.8633	0.01
0.8	0.9614	0.9613	0.01	0.9602	0.12	0.9399	0.9414	0.16	0.9413	0.15	0.925	0.9229	0.23	0.923	0.22
1	1	1	0.00	1	0.00	1	1	0.00	1	0.00	1	1	0.00	1	0.00
Average error %			0.04		0.2			0.11		0.03			0.29		0.4

6. Results and discussion

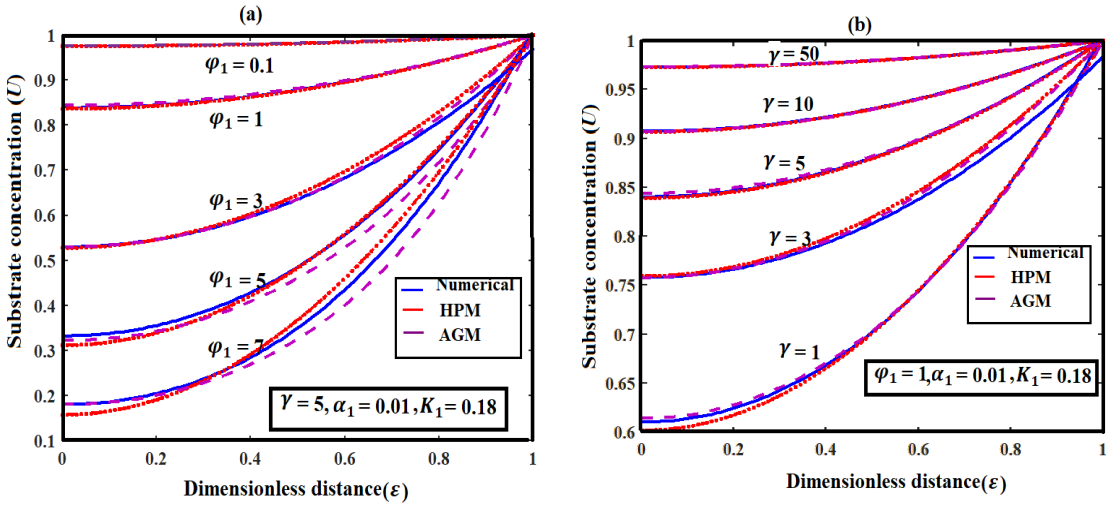

FIGURE 2. Concentration of the substrate (U) against non-dimensional distance (ε) for different parameter values φ_1 and γ using Eqs. (3.1) and (3.5).

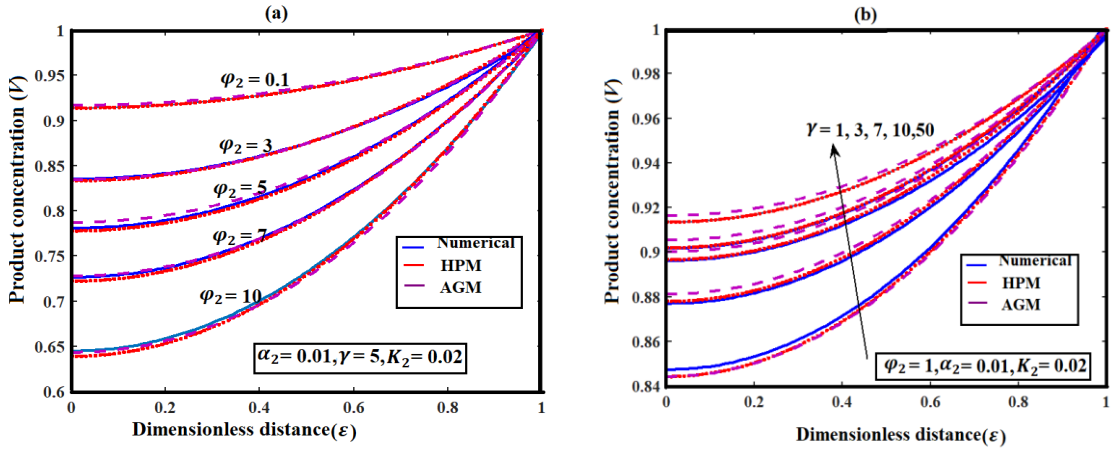

FIGURE 3. Concentration of product (V) against distance (ε) for different values of parameter φ_2 and γ using Eqs. (3.2) and (3.6).

Figures. 2 and 3 display the substrate concentration (U) and product concentration (V) against the non-dimensional distance (ε) for a range of reaction-diffusion (φ_1, φ_2) and saturation parameter γ values using Eqs. (3.1) - (3.2) and Eqs. (3.5) - (3.6). From Figure. 2(a), it is observed that the values of the reaction-diffusion parameter increase $\varphi_1 \left(= \frac{\tilde{R}^2 \tilde{\mu}_{max} \tilde{\Psi} \widetilde{C^c}}{\tilde{Y}_{\frac{X}{S}} D_{Gr}^{\tilde{S}} K_{\tilde{S}}} \right)$, and the

concentration of substrate decreases. An increase in the reaction-diffusion parameter increases the diffusion rate of substrate concentration in the gel-granule $D_{Gr}^{\tilde{S}}$, cell yield $\tilde{Y}_{\frac{X}{S}}$ and monod constant of substrate $K_{\tilde{S}}$. It reduces the catalyst radius $\tilde{R}^2$, maximum growth rate of substrate $\tilde{\mu}_{max}$ and cell density $\Psi\widetilde{C^c}$. In contrast, the hydrogen production rate increases as φ_1 grows because the biological reaction proceeds more quickly than the substrate diffusion. This leads to better substrate consumption and decreased substrate concentration at the gel-granule centre. The substrate concentration does not vary substantially with dimensionless distance and becomes constant when φ_1 is less than or equal to 0.1. It is evident from Figure. 2(b) that an increase in the saturation parameter γ increases the substrate concentration U and decreases the mass transfer in the gel granules and substrate consumption rate. However, a low saturation degree is necessary for the gel granule to attain high mass transfer and substrate consumption. Therefore, the φ_1 and γ should be kept at their maximum and lowest values to achieve greater substrate consumption and, as a result, greater hydrogen production.

According to Figure. 3(a)-3(b), it can be inferred that increasing the value of the reaction-diffusion parameter $\varphi_2$leads to a decrease in product concentration V, and an increase in the values of the saturation parameter γ increases the product concentration V. When φ_2 possesses a small value, the curve becomes a straight line, and the product concentration becomes stable.

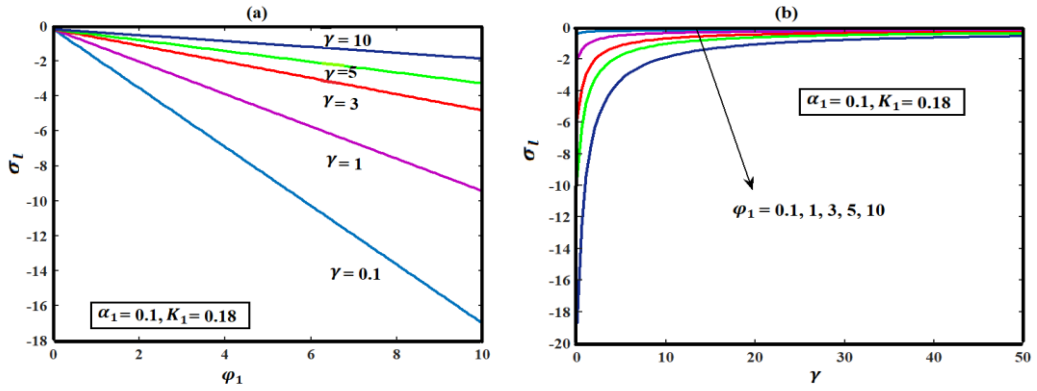

FIGURE 4. The liquid phase's source term σ_l is determined by using Eq. (3.3) and considering reaction-diffusion parameters φ_1 and the saturation value γ.

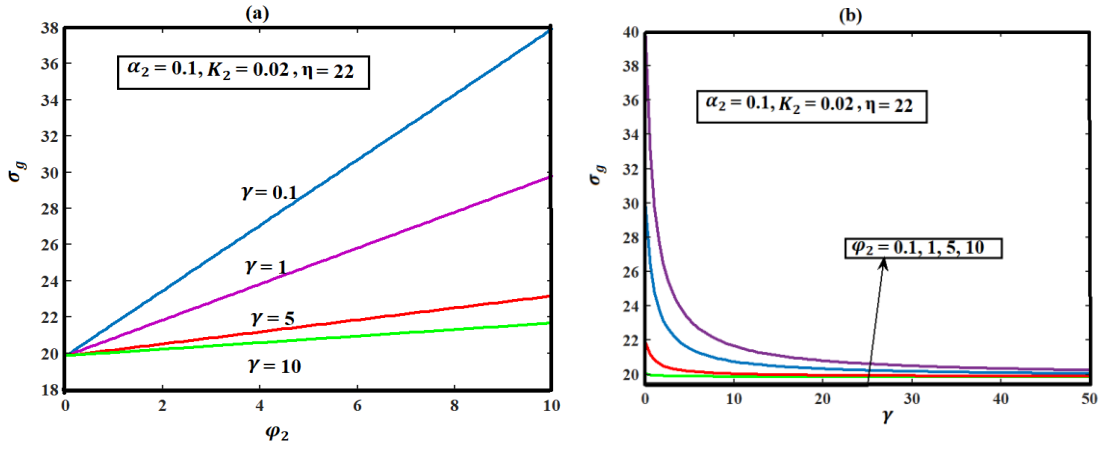

FIGURE 5. Change of the source term gas phase σ_g for various values of parameter a) φ_2, b) γ obtained by Eq. (3.5).

The source term of the liquid σ_l and gas phases σ_g for various parameter values of (φ_1, φ_2) and γ is depicted in Figure. 4(a-b) and Figure. 5(a-b) by applying Eqs. (3.4) and (3.5). It can be noticed from Fig. 4(a-b) that the liquid phase σ_l increases when the values of γ and φ_1 decrease and increase, respectively. As the values of φ_2 decrease and γ increase, the gas phase σ_g decreases. Figure. 5(a-b) supports this inference. Figures. 4 and 5 show that increasing φ_1 and φ_2 values and decreasing γ are necessary to achieve a high mass transfer rate between the gas and liquid phases.

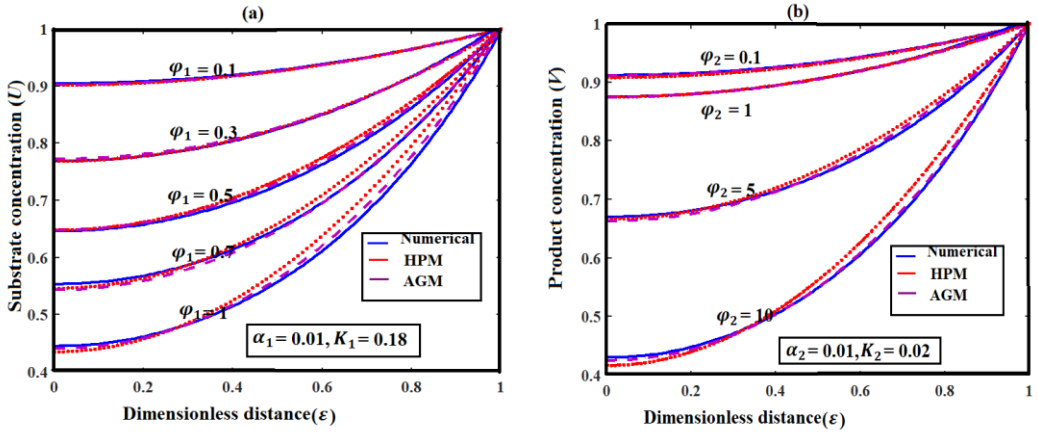

FIGURE 6. Effects of reaction-diffusion parameters (φ_1, φ_2) on a) substrate (U) and b) product concentration (V) for unsaturated enzyme kinetics obtained by Eqs. (4.3) -(4.4) and (4.7) -(4.8).

The dimensionless concentrations U and V for the unsaturated enzyme kinetics limiting case are shown in Figure. 6 for various values of φ_1 and φ_2. From Figure. 6(a-b), it is inferred that the concentration of substrate and product increases when the values of parameters φ_1 and φ_2 decrease, respectively.

7. Conclusion

This work presents a thorough theoretical analysis of multiphase flow transport in the entrapped-cell photobioreactor within the gel granules. The concentration expressions of the substrate, product, and liquid and gas phases were determined analytically using asymptotic methods of homotopy perturbation and the Akbari-Ganji method to solve the non-linear reaction-diffusion equations. The effects of several parameters, including the saturation and reaction-diffusion parameters, were discussed. Furthermore, two limiting situations with saturated and unsaturated enzyme kinetics were given closed-form analytical calculations. The resulting approximation expressions of the concentrations were proved to be highly accurate by direct comparison with dependable numerical data obtained by the MATLAB programme. The proposed solutions can accurately replicate the system's dynamic performance with the parameters, as demonstrated by the close correspondence between the simulated and analytical data. It is helpful to comprehend and forecast the system's behaviour with the expressions provided in this work. It is also a valuable tool for catalyst particle optimization.

8. Appendix A (Homotopy perturbation method)

The homotopy was constructed for the Eqs. (2.7) - (2.8) as follows:

$$(1-P)\left(\frac{d^2U(\varepsilon)}{d\varepsilon^2}+\frac{2}{\varepsilon}\frac{dU(\varepsilon)}{d\varepsilon}\right)+P\left(\frac{d^2U(\varepsilon)}{d\varepsilon}+\frac{2}{\varepsilon}\frac{dU(\varepsilon)}{d\varepsilon}-\frac{1}{K_1}\left[\frac{(\varphi_1)U(\varepsilon)}{(1+\gamma U(\varepsilon))}+\alpha_1\right]\right)=0 \tag{8.1}$$

$$(1-P)\left(\frac{d^2V(\varepsilon)}{d\varepsilon^2}+\frac{2}{\varepsilon}\frac{dV(\varepsilon)}{d\varepsilon}\right)+P\left(\frac{d^2V(\varepsilon)}{d\varepsilon}+\frac{2}{\varepsilon}\frac{dV(\varepsilon)}{d\varepsilon}-\frac{1}{K_2}\left[\frac{(\varphi_2)U(\varepsilon)}{(1+\gamma U(\varepsilon))}+\alpha_2\right]\right)=0 \tag{8.2}$$

The following are the analytical solutions to equations (8.1) and (8.2):

$$U=U_0+PU_1+P^2U_2+\cdots \tag{8.3}$$

$$V=V_0+PV_1+P^2V_2+\cdots \tag{8.4}$$

Using the same powers of p-terms to rearrange the results of substituting Eqs. (8.3) and (8.4) into Eqs. (8.1) and (8.2) can be expressed as:

$$P^0:\frac{d^2U_0}{d\varepsilon^2}+\frac{2}{\varepsilon}\frac{dU_0}{d\varepsilon}=0,\frac{dU_0}{d\varepsilon}(0)=0,U_0(1)=1 \tag{8.5}$$

$$P^0:\frac{d^2V_0}{d\varepsilon^2}+\frac{2}{\varepsilon}\frac{dV_0}{d\varepsilon}=0,\frac{dV_0}{d\varepsilon}(0)=0,V_0(1)=1 \tag{8.6}$$

$$P^1: \frac{d^2U_1}{d\varepsilon^2} + \frac{2}{\varepsilon}\frac{dU_1}{d\varepsilon} - \frac{1}{K_1}\left[\frac{(\varphi_1)U_0}{(1+\gamma U_0)} + \alpha_1\right] = 0, \frac{dU_1}{d\varepsilon}(0) = 0, U_1(1) = 0 \tag{8.7}$$

$$P^1: \frac{d^2V_1}{d\varepsilon^2} + \frac{2}{\varepsilon}\frac{dV_1}{d\varepsilon} - \frac{1}{K_2}\left[\frac{(\varphi_2)U_0}{(1+\gamma U_0)} + \alpha_2\right] = 0, \frac{dV_1}{d\varepsilon}(0) = 0, V_1(1) = 0 \tag{8.8}$$

The following outcomes can be attained by solving equations (8.5) - (8.8):

$$U_0 = 1; V_0 = 1 \tag{8.9}$$

$$U_1 = \frac{(\gamma\alpha_1+\alpha_1+\varphi_1)(\varepsilon^2-1)}{6K_1(1+\gamma)}; V_1 = \frac{(\gamma\alpha_2+\alpha_2+\varphi_2)(\varepsilon^2-1)}{6K_2(1+\gamma)} \tag{8.10}$$

Therefore, the solution can be represented as follows by HPM:

$$U = \lim_{P\to 1} U = U_0 + U_1 = 1 + \frac{(\gamma\alpha_1+\alpha_1+\varphi_1)(\varepsilon^2-1)}{6K_1(1+\gamma)} \tag{8.11}$$

$$V = \lim_{P\to 1} V = V_0 + V_1 = 1 + \frac{(\gamma\alpha_2+\alpha_2+\varphi_2)(\varepsilon^2-1)}{6K_2(1+\gamma)} \tag{8.12}$$

9. Appendix B (Akbari-Ganji method)

It is assumed that the approximate trial solution for equations (2.7) and (2.8) is:

$$U(\varepsilon) = E\cosh(l\varepsilon) + F\sinh(l\varepsilon) \tag{9.1}$$

$$V(\varepsilon) = G\cosh(m\varepsilon) + H\sinh(m\varepsilon) \tag{9.2}$$

Here, *E*, *F*, *G* and *H* are constants. By applying the boundary conditions Eqs. (2.9) – (2.10) in Eqs. (9.1) – (9.2), the values of constants are obtained as:

$$E = \frac{1}{\cosh(l)}, F = 0, G = \frac{1}{\cosh(m)}, H = 0 \tag{9.3}$$

Equation (9.3) is substituted in Eqs. (9.1) – (9.2) to get

$$U(\varepsilon) = \frac{\cosh(l\varepsilon)}{\cosh(l)} \tag{9.4}$$

$$V(\varepsilon) = \frac{\cosh(m\varepsilon)}{\cosh(m)} \tag{9.5}$$

Where l and m are the constant coefficients.

The equations (2.7) – (2.8) can be rearranged in the following manner to get the values of *l* and *m*:

$$f(\varepsilon) = \frac{d^2U(\varepsilon)}{d\varepsilon^2} + \frac{2}{\varepsilon}\frac{dU(\varepsilon)}{d\varepsilon} - \frac{1}{K_1}\left[\frac{(\varphi_1)U(\varepsilon)}{(1+\gamma U(\varepsilon))} + \alpha_1\right] = 0 \tag{9.6}$$

$$g(\varepsilon) = \frac{d^2V(\varepsilon)}{d\varepsilon^2} + \frac{2}{\varepsilon}\frac{dV(\varepsilon)}{d\varepsilon} - \frac{1}{K_2}\left[\frac{(\varphi_2)U(\varepsilon)}{(1+\gamma U(\varepsilon))} + \alpha_2\right] = 0 \tag{9.7}$$

Equations (9.6) - (9.7) can be expressed as follows when the equations (9.4) and (9.5) have been substituted in equations (9.6) -(9.7) and at $\varepsilon = 1$.

$$f(1) = l^2 + 2\,l\tanh(l) - \frac{1}{K_1}\left[\frac{\varphi_1}{(1+\gamma)} + \alpha_1\right] = 0 \tag{9.8}$$

$$g(1) = m^2 + 2\,m\tanh(m) - \frac{1}{K_2}\left[\frac{(\varphi_2)}{(1+\gamma)} + \alpha_2\right] = 0 \tag{9.9}$$

By solving the above two equations, we can obtain the values of the constant coefficients l and m.

Conflicts of Interest: The authors declare that there are no conflicts of interest regarding the publication of this paper.

References

[1] M.Y. Azwar, M.A. Hussain, A.K. Abdul-Wahab, Development of Biohydrogen Production by Photobiological, Fermentation and Electrochemical Processes: A Review, Renew. Sustain. Energy Rev. 31 (2014), 158-173. https://doi.org/10.1016/j.rser.2013.11.022.

[2] M.D. Redwood, R.L. Orozco, A.J. Majewski, L.E. Macaskie, An Integrated Biohydrogen Refinery: Synergy of Photofermentation, Extractive Fermentation and Hydrothermal Hydrolysis of Food Wastes, Bioresource Technol. 119 (2012), 384-392. https://doi.org/10.1016/j.biortech.2012.05.040.

[3] Y. Luo, W. Guo, H.H. Ngo, L.D. Nghiem, F.I. Hai, J. Zhang, S. Liang, X.C. Wang, A Review on the Occurrence of Micropollutants in the Aquatic Environment and Their Fate and Removal During Wastewater Treatment, Sci. Total Environ. 473–474 (2014), 619–641. https://doi.org/10.1016/j.scitotenv.2013.12.065.

[4] P. Prachanurak, C. Chiemchaisri, W. Chiemchaisri, K. Yamamotob, Biomass Production from Fermented Starch Wastewater in Photo-Bioreactor with Internal Overflow Recirculation, Bioresource Technol. 165 (2014), 129–136. https://doi.org/10.1016/j.biortech.2014.03.119.

[5] Q. Li, B. Guo, J. Yu, J. Ran, B. Zhang, H. Yan, J.R. Gong, Highly Efficient Visible-Light-Driven Photocatalytic Hydrogen Production of CdS-Cluster-Decorated Graphene Nanosheets, J. Amer. Chem. Soc. 133 (2011), 10878–10884. https://doi.org/10.1021/ja2025454.

[6] Y.Z. Wang, Q. Liao, X. Zhu, R. Chen, C.L. Guo, J. Zhou, Bioconversion Characteristics of Rhodopseudomonas Palustris CQK 01 Entrapped in a Photobioreactor for Hydrogen Production, Bioresource Technol. 135 (2013), 331–338. https://doi.org/10.1016/j.biortech.2012.09.105.

[7] Y.Z. Wang, Q. Liao, X. Zhu, X. Tian, C. Zhang, Characteristics of Hydrogen Production and Substrate Consumption of Rhodopseudomonas Palustris CQK 01 in an Immobilized-Cell Photobioreactor, Bioresource Technol. 101 (2010), 4034–4041. https://doi.org/10.1016/j.biortech.2010.01.045.

[8] C. Zhang, A.J. Wang, Q.G. Zhang, A Two-Dimensional Mass Transfer Model for an Annular Bioreactor Using Immobilized Photosynthetic Bacteria for Hydrogen Production, Biotechnol. Lett. 35 (2013), 1579–1587. https://doi.org/10.1007/s10529-013-1250-2.

[9] C. Zhang, H. Zhang, Z. Zhang, Y. Jiao, Q. Zhang, Effects of Mass Transfer and Light Intensity on Substrate Biological Degradation by Immobilized Photosynthetic Bacteria Within an Annular Fiber-Illuminating Biofilm Reactor, J. Photochem. Photobiol. B: Biol. 131 (2014), 113–119. https://doi.org/10.1016/j.jphotobiol.2014.01.015.

[10] Y. Yang, Q. Liao, X. Zhu, H. Wang, R. Wu, D.J. Lee, Lattice Boltzmann Simulation of Substrate Flow Past a Cylinder with PSB Biofilm for Bio-Hydrogen Production, Int. J. Hydrogen Energy. 36 (2011), 14031–14040. https://doi.org/10.1016/j.ijhydene.2011.04.026.

[11] Q. Liao, D.-M. Liu, D.-D. Ye, X. Zhu, D.-J. Lee, Mathematical modeling of two-phase flow and transport in an immobilized-cell photobioreactor, Int. J. Hydrogen Energy. 36 (2011), 13939–13948. https://doi.org/10.1016/j.ijhydene.2011.03.088.

[12] C.L. Guo, H.S. Pei, H.X. Cao, F.Q. Guo, D.M. Liu, Y.M. Li, Simulation on Characteristics of Photo-Hydrogen Production and Substrate Degradation under Various Stacking Types, Int. J. Hydrogen Energy. 40 (2015), 10401–10409. https://doi.org/10.1016/j.ijhydene.2015.06.152.

[13] D.D. Ganji, N. Ranjbar Malidarreh, M. Akbarzade, Comparison of Energy Balance Period with Exact Period for Arising Nonlinear Oscillator Equations, Acta Appl. Math. 108 (2008), 353–362. https://doi.org/10.1007/s10440-008-9315-2.

[14] S.Z. Shirejini, M. Fattahi, Mathematical Modeling and Analytical Solution of Two-Phase Flow Transport in an Immobilized-Cell Photo Bioreactor Using the Homotopy Perturbation Method (HPM), Int. J. Hydrogen Energy. 41 (2016), 18405–18417. https://doi.org/10.1016/j.ijhydene.2016.08.055.

[15] T. Praveen, L. Rajendran, Theoretical Analysis Through Mathematical Modeling of Two-Phase Flow Transport in an Immobilized-Cell Photobioreactor, Chem. Phys. Lett. 625 (2015), 193–201. https://doi.org/10.1016/j.cplett.2015.01.007.

[16] V.S. Sajja, B. Sripathy, A Spectral Method to Reaction-Diffusion Equations in Gel Granules Using Bernoulli Wavelets, Int. J. Pure Appl. Math. 118 (2018), 301-310.

[17] A. Meena, L. Rajendran, Analytical Solution of System of Coupled Non-Linear Reaction Diffusion Equations. Part I: Mediated Electron Transfer at Conducting Polymer Ultramicroelectrodes, J. Electroanal. Chem. 647 (2010), 103–116. https://doi.org/10.1016/j.jelechem.2010.06.013.

[18] P. Jeyabarathi, M. Abukhaled, M. Kannan, L. Rajendran, M.E.G. Lyons, New Analytical Expressions of Concentrations in Packed Bed Immobilized-Cell Electrochemical Photobioreactor, Electrochem. 4 (2023), 447–459. https://doi.org/10.3390/electrochem4040029.

[19] C.L. Guo, H.X. Cao, H.S. Pei, F.Q. Guo, D.-M. Liu, A Multiphase Mixture Model for Substrate Concentration Distribution Characteristics and Photo-Hydrogen Production Performance of the Entrapped-Cell Photobioreactor, Bioresource Technol. 181 (2015), 40–46. https://doi.org/10.1016/j.biortech.2015.01.022.

[20] H. Koku, Aspects of the Metabolism of Hydrogen Production by Rhodobacter Sphaeroides, Int. J. Hydrogen Energy. 27 (2002), 1315–1329. https://doi.org/10.1016/s0360-3199(02)00127-1.

[21] L.C. Mary, R.U. Rani, A. Meena, L. Rajendran, Nonlinear Mass Transfer at the Electrodes with Reversible Homogeneous; Reactions: Taylor's Series and Hyperbolic Function Method, Int. J. Electrochem. Sci. 16 (2021), 151037. https://doi.org/10.20964/2021.01.73.

[22] K. Nirmala, B. Manimegalai, L. Rajendran, Steady-State Substrate and Product Concentrations for Non-Michaelis-Menten Kinetics in an Amperometric Biosensor –Hyperbolic Function and Padé Approximants Method, Int. J. Electrochem. Sci. 15 (2020), 5682–5697. https://doi.org/10.20964/2020.06.09.

[23] R. Usha Rani, L. Rajendran, M.E.G. Lyons, Steady-State Current in Product Inhibition Kinetics in an Amperometric Biosensor: Adomian Decomposition and Taylor Series Method, J. Electroanal. Chem. 886 (2021), 115103. https://doi.org/10.1016/j.jelechem.2021.115103.

[24] S. Vinolyn Sylvia, R. Joy Salomi, L. Rajendran, M. Abukhaled, Solving Nonlinear Reaction–Diffusion Problem in Electrostatic Interaction with Reaction-Generated pH Change on the Kinetics of Immobilized Enzyme Systems Using Taylor Series Method, J. Math. Chem. 59 (2021), 1332–1347. https://doi.org/10.1007/s10910-021-01241-7.

[25] A.M. Wazwaz, A Reliable Modification of Adomian Decomposition Method, Appl. Math. Comp. 102 (1999), 77–86. https://doi.org/10.1016/s0096-3003(98)10024-3.

[26] K. Ranjani, R. Swaminathan, S.G. Karpagavalli, Mathematical Modelling of a Mono-Enzyme Dual Amperometric Biosensor for Enzyme-Catalyzed Reactions Using Homotopy Analysis and Akbari-Ganji Methods, Int. J. Electrochemi. Sci. 18 (2023), 100220. https://doi.org/10.1016/j.ijoes.2023.100220.

[27] M. Abukhaled, Variational Iteration Method for Nonlinear Singular Two-Point Boundary Value Problems Arising in Human Physiology, J. Math. 2013 (2013), 720134. https://doi.org/10.1155/2013/720134.

[28] J.H. He, Homotopy Perturbation Technique, Comp. Meth. Appl. Mech. Eng. 178 (1999), 257–262. https://doi.org/10.1016/s0045-7825(99)00018-3.

[29] J.H. He, A Coupling Method of a Homotopy Technique and a Perturbation Technique for Non-Linear Problems, Int. J. Non-Linear Mech. 35 (2000), 37–43. https://doi.org/10.1016/s0020-7462(98)00085-7.

[30] R. Swaminathan, K. Venugopal, M. Rasi, M. Abukhaled, L. Rajendran, Analytical Expressions for the Concentration and Current in the Reduction of Hydrogen Peroxide at a Metal-Dispersed Conducting Polymer Film, Quim. Nova. 43 (2020), 58–65. https://doi.org/10.21577/0100-4042.20170454.

[31] R. Swaminathan, M. Chitra Devi, L. Rajendran, K. Venugopal, Sensitivity and Resistance of Amperometric Biosensors in Substrate Inhibition Processes, J. Electroanal. Chem. 895 (2021), 115527. https://doi.org/10.1016/j.jelechem.2021.115527.

[32] S.V. Sylvia, R.J. Salomi, L. Rajendran, M.E.G. Lyons, Amperometric Biosensors and Coupled Enzyme Nonlinear Reactions Processes: A Complete Theoretical and Numerical Approach, Electrochimica Acta. 415 (2022), 140236. https://doi.org/10.1016/j.electacta.2022.140236.

[33] A. Reena, SG. Karpagavalli, L. Rajendran, B. Manimegalai, R. Swaminathan, Theoretical Analysis of Putrescine Enzymatic Biosensor with Optical Oxygen Transducer in Sensitive Layer Using Akbari–Ganji Method, Int. J. Electrochem. Sci. 18 (2023), 100113. https://doi.org/10.1016/j.ijoes.2023.100113.

[34] A. Nebiyal, R. Swaminathan, SG. Karpagavalli, Reaction Kinetics of Amperometric Enzyme Electrode in Various Geometries Using the Akbari-Ganji Method, Int. J. Electrochem. Sci. 18 (2023), 100240. https://doi.org/10.1016/j.ijoes.2023.100240.

[35] A. Reena, SG. Karpagavalli, R. Swaminathan, Theoretical Analysis and Steady-State Responses of the Multienzyme Amperometric Biosensor System for Nonlinear Reaction-Diffusion Equations, Int. J. Electrochem. Sci. 18 (2023), 100293. https://doi.org/10.1016/j.ijoes.2023.100293.